

Inverted and Inclined Climbing Using Capillary Adhesion in a Quadrupedal Insect-Scale Robot

Yufeng Chen , Neel Doshi , and Robert J. Wood 

Abstract—Many insects demonstrate remarkable locomotive capabilities on inclined or even inverted surfaces. Achieving inverted locomotion is a challenge for legged insect-scale robots because repeated attachment and detachment to a surface usually requires the design of special climbing gaits, adhesion mechanisms, sensing, and feedback control. In this study, we propose a novel adhesion method that leverages capillary and lubrication effects to achieve simultaneous adhesion and sliding. We design a 47 mg adhesion pad and install it on a 1.4 g insect-scale quadrupedal robot to demonstrate locomotion on inverted and inclined surfaces. On an inverted acrylic surface, the robot's climbing and turning speeds are 0.3 cm/s and 23.6 °/s, respectively. Further, the robot can climb a 30° inclined acrylic surface at 0.04 cm/s. This light-weight, passively stable, and versatile adhesion design is suitable for insect-scale robots with limited sensing, actuation, and control capabilities.

Index Terms—Micro/nano robots, mechanism design, biologically-inspired robots.

I. INTRODUCTION

MANY animal species demonstrate remarkable locomotive capabilities such as climbing on steep inclines, tree trunks, and overhanging tree branches. In particular, insects and arachnids such as ants [1], caterpillars, and spiders can climb along complex surfaces because of the diminishing inertia and dominating surface effects at the millimeter scale. Previous studies on animal adhesion identified two major mechanisms: gecko-like dry adhesion based on Van der Waals interactions [2], [3] and wet adhesion based on capillary effects [4], [5].

Legged robots that can adhere to and move along inclined or inverted surfaces are suitable for a wide range of applications such as inspecting the inside of complex engines and

Manuscript received February 23, 2020; accepted June 6, 2020. Date of publication June 19, 2020; date of current version June 30, 2020. This letter was recommended for publication by Associate Editor Barbara Mazzolai and Editor Xinyu Liu upon evaluation of the reviewers' comments. This work was supported in part by the Research Laboratory of Electronics at MIT and in part by the Wyss Institute for Biologically Inspired Engineering. (Corresponding author: Yufeng Chen.)

Yufeng Chen is with the Soft and Microrobotics Lab, Department of Electrical Engineering and Computer Science, and the Research Laboratory of Electronics, Massachusetts Institute of Technology, Cambridge, MA 02139 USA (e-mail: yufengc@mit.edu).

Neel Doshi is with the Department of Mechanical Engineering, Massachusetts Institute of Technology, Cambridge, MA 02139 USA (e-mail: nddoshi@mit.edu).

Robert J. Wood is with the Harvard Microrobotics Lab, School of Engineering and Applied Sciences, Harvard University and the Wyss Institute of Biological Engineering, Cambridge, MA 02138 USA (e-mail: rjwood@eecs.harvard.edu).

This letter has supplementary downloadable material available at <https://ieeexplore.ieee.org>, provided by the authors.

Digital Object Identifier 10.1109/LRA.2020.3003870

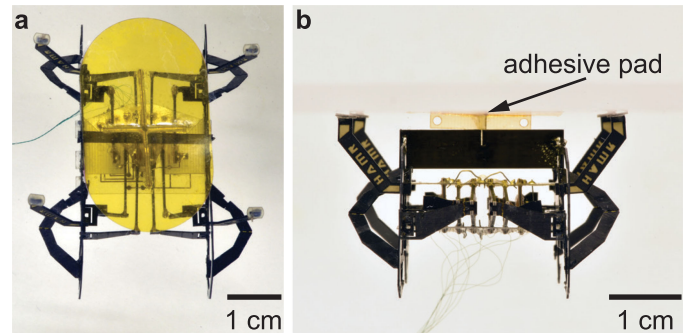


Fig. 1. Top view (a) and front view (b) images of an insect-scale quadrupedal robot that is attached inverted to an acrylic surface through capillary adhesion. The robot weighs 1.4 gram, and its length, width, and height are 4 cm \times 2 cm \times 2 cm, respectively. The compliant adhesion pad weighs 47 mg.

search-and-rescue in unstructured environments. Inspired by biological examples, several climbing robots [6]–[10] have been developed to demonstrate locomotion on inclined or inverted surfaces. In addition to using bio-inspired adhesion methods, robotic systems also utilize electrostatic [11], magnetic [12], [13], vacuum [14], [15], and capillary-based [16] mechanisms.

There are two major challenges in designing legged climbing robots: 1) achieving repeatable foot attachment and detachment from the substrate during locomotion; and 2) developing gaits or controllers that can stabilize the robot's center-of-mass (COM) motion. Several adhesion designs have been developed to address these challenges for climbing robots of different weight and sizes. At a larger scale (>50 g, >10 cm), dry adhesion and vacuum-based adhesion are advantageous because these methods can generate large areal force density and they can be applied to different types of surfaces. However, these mechanisms are either heavy (>5 g) or require a pump, and they sometimes require the robot legs to engage the surface at a specific orientation and with a well-controlled preload force. These requirements are difficult to satisfy in micro-scale robots (<5 g, <10 cm) because these vehicles have limited payload and actuated degrees-of-freedom (DOFs). Lightweight (<0.1 g) electrostatic adhesion [9], [17] mechanisms become advantageous in micro-scale systems. Although electrostatic adhesion has lower areal force density compared to vacuum-based methods, they are sufficient for micro-scale robots because these systems have large surface area to weight ratio. However, electrostatic adhesion [18] remains challenging at the micro-scale because it requires a high driving voltage (>200 V), it is sensitive to surface

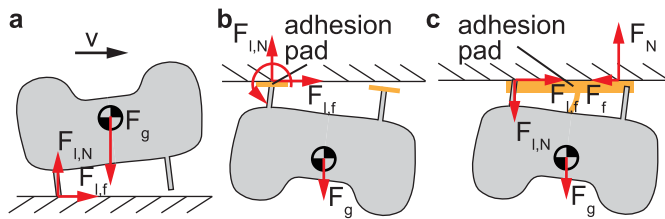


Fig. 2. Comparison between walking upright versus walking inverted. (a) A free body diagram of a robot walking upright on a level surface. The robot is passively stable due to the restoring body torque contributed by the normal force $F_{l,N}$ with respect to the robot COM. (b) A free body diagram of a robot walking inverted on a surface. To maintain stability, the adhesion pad at the robot's rear foot needs to generate an upward adhesion force and a restoring body torque that counteracts the destabilizing torque from the robot weight. (c) A free body diagram of an alternative inverted locomotion design. An adhesion pad that can generate large normal force (F_N) and a small friction force (F_f) is attached to the robot chassis.

properties (e.g., conductivity and roughness), and it requires sensing and feedback [9] to achieve reliable and repeatable foot attachment and detachment. To demonstrate effective locomotion on inverted or inclined surfaces in micro-scale robots, we seek a novel lightweight adhesion design that does not require complex gait designs, sensing, and closed-loop feedback.

In this study, we demonstrate inverted-climbing in a 1.4 g quadrupedal microrobot through leveraging the principles of capillary adhesion and lubrication. The robot adheres to an inclined or inverted surface by using the capillary adhesion force between a wetted thin pad and the desired surface. Fig. 1(a) and (b) show top view and side view images of this robot hanging from an acrylic surface, respectively. While attached, the robot can move along the surface because the thin water film between the two surfaces significantly reduces friction to enable slipping between the pad and the surface. The main contribution of this work is the development of an inverted climbing mechanism that modifies the relative magnitude of normal and friction forces. This design does not require repeated leg attachment and detachment and allows the robot to move along an inverted surface at 0.3 cm/s (0.08 body length/s). In addition, it can make left or right turns at $23.6^\circ/s$ and $18.1^\circ/s$, respectively.

II. DESIGN OF INVERTED LOCOMOTION AND A MODEL OF WET ADHESION

When a legged robot walks on a level surface in an upright orientation, its feet repeatedly make contact with the ground and push the robot forward. Each foot contact is associated with a normal force and a friction force and they must satisfy the friction cone condition ($F_{l,f} \leq \mu F_{l,N}$) to avoid slipping. We use $F_{l,f}$ and $F_{l,N}$ to denote the magnitude of friction and normal forces from the robot leg, respectively. In addition, the robot needs to maintain upright stability as one or more of its legs lift off the ground. Fig. 2(a) illustrates a robot walking on a horizontal surface. In this example, the restoring torque generated by the normal ($F_{l,N}$) and the friction ($F_{l,f}$) forces makes the robot passively stable—it does not need to sense and actively control its leg motion to maintain stability.

Locomotion on an inverted surface is challenging because the robot leg contact condition and robot stability change. Fig. 2(b) shows the free body diagram of a robot walking on an inverted surface. Each robot foot is equipped with an adhesion pad. When the robot's front leg lifts off the surface, the adhesion pad at the rear foot needs to generate an upward force that balances the robot weight. In addition, it needs to generate a counterclockwise torque that counteracts the destabilizing torque from the robot weight at the robot's COM. This requires the foot pad to be resilient against peeling. A previous work [9] that used electrostatic adhesion required the adhesive foot pads to repeatedly attach and detach from the surface. The stability of the robot is then sensitive to the pre-load force and the position of the leg with respect to the robot COM. That work found that the robot cannot walk on an inverted surface indefinitely without sensing (i.e., to detect proper or incorrect attachment) and feedback.

To avoid repeated attachment and detachment, Fig. 2(c) illustrates an alternative design in which the adhesion mechanism and robot legs are independent. In this design, the adhesion mechanism (the orange colored region in Fig. 2(c)) always remains attached to the surface while the legs move cyclically under a typical walking gait. The adhesion mechanism generates a large upward force (F_N) but very small friction force (F_f) such that the mechanism can slide along the surface while attached. This design is advantageous because robot locomotion becomes passively stable — the adhesion mechanism remains attached and generates stabilizing forces and torques.

To generate a large normal force (F_N) and a small friction force (F_f) during inverted locomotion, we design an adhesion mechanism that leverages capillary and lubrication effects. As illustrated in Fig. 3(a), a thin layer of water is placed between the inverted surface and the adhesion surface (orange). The fluid motion and associated forces are described by the Navier Stokes equation:

$$\rho \left(\frac{\partial \mathbf{u}}{\partial t} + \mathbf{u} \cdot \nabla \mathbf{u} \right) = -\nabla p + \mu \nabla^2 \mathbf{u} + \nabla \cdot \boldsymbol{\sigma}_f, \quad (1)$$

where ρ , \mathbf{u} , p , μ , and $\boldsymbol{\sigma}_f$ represent fluid density, velocity field, pressure field, viscosity, and surface tension stress tensor, respectively. This equation does not have a closed-form solution and consequently we analyze this problem under two regimes: surface tension dominated flow (Fig. 3(a)–(b)) and fluid inertia dominated flow (Fig. 3(c)–(d)). In the following derivation, we make several simplifying assumptions:

- 1) The adhesion pad is a circle of radius R
- 2) The adhesion pad is parallel to the attached surface and the water film thickness is constant
- 3) The adhesion pad does not deform under disturbances and we do not model peeling

When the robot walks at a very low speed (< 1 cm/s), surface tension dominates and the governing equation reduces to a static equation:

$$\nabla p = \nabla \cdot \boldsymbol{\sigma}_f. \quad (2)$$

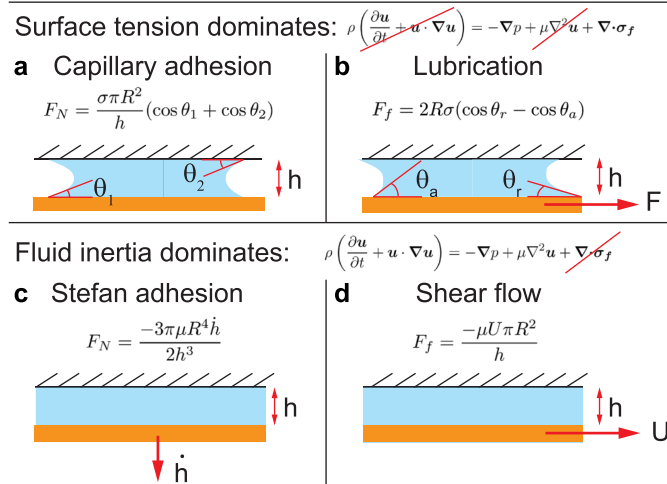


Fig. 3. Simplifying analytical solutions that describe capillary adhesion and lubrication effects. (a) Upward adhesion force due to fluid surface tension. (b) Friction force due to fluid surface tension. In (a) and (b), we assume the adhesion pad moves slowly (< 1 cm/s) such that the surface tension contribution is larger than fluid viscous and inertial effects. (c) Upward restoring force when the adhesion pad is pulled away from the surface at a speed \dot{h} . (d) Damping force when the adhesion pad is pulled tangentially along the surface at a speed U . In (c) and (d), we assume the disturbances generate a large instantaneous speed (> 2 cm/s) such that fluid viscosity and inertia become dominating factors compared to static surface tension.

Based on the first two assumptions, the analytical solutions of the normal and shear forces are given by:

$$\begin{aligned} F_N &= \frac{\sigma \pi R^2}{h} (\cos \theta_1 + \cos \theta_2) \\ F_f &= 2R\sigma(\cos \theta_r - \cos \theta_a) \end{aligned} \quad (3)$$

Here σ is the surface tension coefficient, h is the water film thickness, and θ_1 and θ_2 are the contact angles at the adhesion pad and the inverted surface, respectively. In addition, θ_r and θ_a are the receding and advancing contact angles when the pad is pulled with a shear force F . Unlike θ_1 and θ_2 that represent the equilibrium contact angles at the liquid-solid interface, θ_r and θ_a result from an external pulling force F that is indicated in Fig. 3(b). Due to the induced shear stress at the liquid-solid contact line, the contact angle changes. This difference between θ_r and θ_a causes a small resistive force F_f that opposes the pulling force F . The ratio between the normal and friction forces is given by:

$$\frac{F_N}{F_f} = \frac{\pi R \cos \theta_1 + \cos \theta_2}{2h \cos \theta_r - \cos \theta_a} \propto \frac{R}{h}. \quad (4)$$

At the static limit, equation (4) shows the ratio F_N/F_f can be significantly larger than one because the pad radius R and the water film thickness h are on the order of 5–10 mm and 10–100 μm , respectively. This result implies that capillary adhesion and lubrication effects can allow an adhesion pad to slide along a surface while remaining attached.

Furthermore, this mechanism design is resilient against disturbances at the dynamic limit where fluid inertia dominates (Fig. 3(c)–(d)). In this limit, the surface tension term is ignored

and the governing equation reduces to:

$$\rho \left(\frac{\partial \mathbf{u}}{\partial t} + \mathbf{u} \cdot \nabla \mathbf{u} \right) = -\nabla p + \mu \nabla^2 \mathbf{u}. \quad (5)$$

If the adhesion pad is suddenly pulled away from the attaching surface along its normal direction (Fig. 3(c)), the normal velocity \dot{h} increases. Since water is incompressible, it flows under the adhesion pad and this flow creates an upward restoring force. This upward force is known as Stefan adhesion and its analytical form is given by:

$$F_N = \frac{-3\pi\mu R^4 \dot{h}}{2h^3}. \quad (6)$$

Similarly, if the adhesion pad is suddenly pulled along a direction tangential to the attaching surface, the fluid viscosity creates a shear force opposing the direction of motion U . The analytical solution of shear flow is given by:

$$F_f = \frac{-\mu U \pi R^2}{h}. \quad (7)$$

The cases illustrated by Fig. 3(c)–(d) show how this mechanism is robust against disturbances in both the normal and shear directions. Hence, through exploiting capillary and lubrication effects, the adhesion pad can maintain strong and robust attachment while permitting sliding motion along the tangential directions.

III. EXPERIMENTAL SETUP, RESULTS, AND DISCUSSION

A. Design of Adhesion Experiments

To validate the proposed adhesion method based on surface tension, we design and conduct three sets of experiments. First, we measure the normal and the shear forces and compare these measurements with theoretical predictions made in the previous section. Second, we design adhesion mechanisms for a quadrupedal insect-scale robot and demonstrate adhesion robustness in a passive robot model. Third, we install the adhesion mechanism on an actuated robot to demonstrate locomotion on inverted and inclined surfaces.

B. Static Force Measurement of Adhesion Mechanisms

The previous section proposes the design of a novel adhesion mechanism that can adhere to a surface while sliding along it tangentially. Concurrent adhesion and sliding is enabled by having a large ratio of normal to friction force (equation 4). Here we design experiments to validate this relationship. As shown in Fig. 4(a) and (b), we measure the maximum normal (F_N) and shear (F_f) force by using centimeter-scale adhesion pads. The maximum force is defined as the critical weight at which the adhesion fails ($F_{N,\text{max}}$) or when the pad starts to slide ($F_{f,\text{max}}$).

The first iteration of our design uses a 160 μm thick glass slide (VWR micro cover glass) that has an area of 18 mm \times 18 mm (Fig. 4(c)). We chose a glass surface because it is flat, rigid, and hydrophilic ($\cos \theta \approx 0^\circ$) [19]. These properties imply a glass adhesion pad can generate a large normal force (F_N). Since this adhesion pad is square instead of circular, we modify

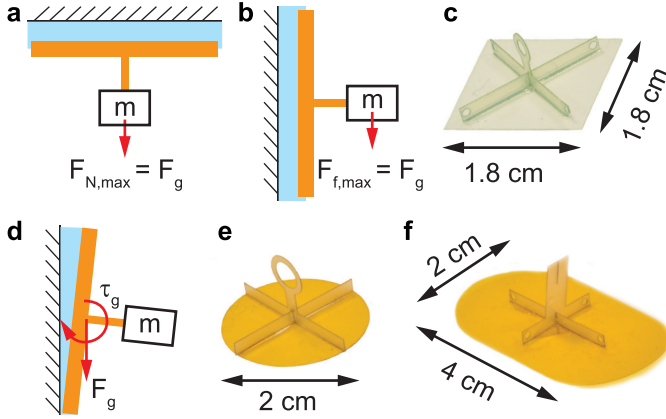


Fig. 4. Design of adhesion experiments and adhesion mechanisms. (a) An illustration showing the normal force measurement. (b) An illustration showing the friction force measurement. (c) An image of the square glass adhesion pad. (d) The torque induced by the pulling weight causes the adhesion pad to tilt, and this increases the sliding friction. (e) An image of a circular polyimide (Kapton) adhesion pad. (f) An image of a compliant polyimide adhesion pad that is used in all robot adhesion experiments.

TABLE I
MODELS AND EXPERIMENTS OF STATIC CAPILLARY ADHESION. ROWS 1–6
SHOW THE MODEL PARAMETERS, AND ROWS 7–8 COMPARE THE
MODEL PREDICTIONS WITH MEASUREMENTS

	Glass		Polyimide (Kapton)	
	Model	Exp	Model	Exp
θ_1	0°	-	56°	-
θ_2	0°	-	0°	-
θ_r	0°	-	45°	-
θ_a	30°	-	76°	-
h	100 μm	-	100 μm	-
σ	72.9 $\text{mN}\cdot\text{m}^{-1}$	-	72.9 $\text{mN}\cdot\text{m}^{-1}$	-
F_N	470 mN	490 mN	360 mN	78 mN
F_f	0.35 mN	4 mN	0.68 mN	4.9 mN

equation (3) to obtain approximative solutions:

$$\begin{aligned} F_N &= \frac{\sigma l^2}{h} (\cos \theta_1 + \cos \theta_2) \\ F_f &= 2l\sigma (\cos \theta_r - \cos \theta_a) \end{aligned} \quad (8)$$

Here l denotes the length of the square adhesion pad and it has a value of 18 mm. The glass adhesion pad adheres to a glass surface, and this implies the contact angles (θ_1 and θ_2) at both interfaces have the same value. The values of all model parameters are shown in the first column of Table I. The measured adhesion and shear forces are 490 mN and 4 mN (Table I, column 2, rows 7–8), respectively. While the normal force measurement agrees well with equation (8), the measured friction force is approximately 10 times larger than the prediction from equation (8). This discrepancy is mainly contributed by the sliding friction between the adhesion pad and the surface due to the torque (τ_g) exerted by the pulling mass. As illustrated by Fig. 4(d), this violates our second assumption that states the water film thickness is constant. Despite having this discrepancy,

we measure the normal to friction force ratio to be larger than 120, which proves that the sliding adhesion design is feasible.

However, it is undesirable to install a glass adhesion pad on an insect-scale robot because it is heavy (240 mg) and rigid. The robot has a limited payload, and more importantly it is advantageous to have a compliant adhesion mechanism such that the robot can conform to local deformation and walk on curved surfaces. Fig. 4(e) and (f) show two adhesion pads made of 25 μm thick polyimide (Kapton) adhesion surfaces and 130 μm thick fiber glass support structures. The adhesion pad in Fig. 4(e) weighs 36 mg (0.35 mN) and it has a diameter of 2 cm. We use equation (3) to estimate its adhesion and friction forces, and we list the values of model parameters in the third column of Table I. We model the polyimide adhesion pad being attached to a glass surface, which implies the contact angles at the two interfaces (θ_1 and θ_2) are different. The values of static, receding, and advancing contact angles of water on polyimide are taken from existing literature [20], [21]. We further compare this model prediction with experimental measurement in the fourth column of Table I, and we find the maximum measured normal and friction forces are 78 mN and 4.9 mN, respectively. The maximum normal force is substantially smaller than the model prediction and the normal force of the glass adhesion pad because the polyimide pad is compliant and consequently it deforms when a local failure occurs. The friction force is similar to that of the glass adhesion pad, and it is approximately seven times larger than the model prediction. Similar to the glass adhesion pad, we believe this discrepancy is caused by the tilting of the adhesion pad (Fig. 4(d)). Although the polyimide adhesion pad's compliance and tilting substantially change the normal and friction forces, our experiment shows the normal to friction force ratio is larger than 15. This implies the robot can demonstrate simultaneous adhesion and sliding by using a lightweight polyimide adhesion mechanism. In these experiments, we estimate the water film thickness to be approximately 100 μm based on the amount of water we put on the adhesion pad.

Our experiment further demonstrates that the friction force varies significantly depending on the water film thickness. Since the polyimide pad is compliant, regions of vacuum may form if there is an insufficient amount of water between the pad and the surface. As the adhesion pad is pulled along a surface, the water film gradually thins out and it leads to a large increase in friction. With less water for adhesion, the maximum friction force can increase to 34 mN before adhesion fails.

C. Adhesion Experiments With a Static Robot Model

In this work, we aim to demonstrate inverted locomotion with the 1.4 g (13.7 mN) Harvard Ambulatory MicroRobot (HAMR) [22]. To enable inverted locomotion, the normal and friction forces generated by the adhesion pad need to satisfy the following conditions [23]:

$$\begin{aligned} F_N &> (m_{\text{robot}} + m_{\text{payload}})g \\ F_f &< \min(4\mu F_{\text{blocked}}, 4F_{\text{thrust}}) \end{aligned} \quad (9)$$

where μ is the friction coefficient, F_{blocked} and F_{thrust} are the normal and tangential blocked force of each robot leg. This

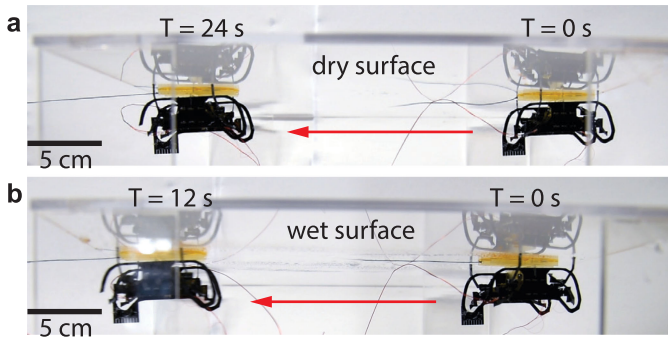


Fig. 5. Pulling demonstration on an inverted acrylic surface. (a) A robot model is pulled along a horizontal surface while it remains attached through capillary adhesion. The robot is pulled at a speed of 0.6 cm/s on a dry surface. (b) The same pulling experiment is conducted on a wetted surface at a speed of 1.2 cm/s.

means the friction force has to be less than the maximum force generated by the robot during locomotion. For a HAMR, F_{blocked} and F_{thrust} are 17.7 mN and 13.0 mN [22].

Given the robot mass, we aim to design an adhesion pad that can generate over 50 mN of normal force and less than 10 mN of friction force. Fig. 4(f) shows an adhesion pad with a mass of 47 mg (0.46 mN) that has approximately twice the area of the one shown in Fig. 4(e). The estimated normal and friction forces are 150 mN and 10 mN, respectively. Given that the maximum friction force satisfies equation (9), having a larger adhesion surface area is beneficial for inverted locomotion for the following reasons. First, a larger adhesion pad carries a larger amount of water, and this implies the robot can walk for a longer distance before the water film area substantially shrinks and reduces adhesion. The robot leaves a water trace as it moves along a surface and consequently the water film slowly thins out due to a combination of fluid viscosity, non-slip boundary condition, and surface roughness. Assuming the water film has a constant thickness of $50 \mu\text{m}$, the adhesion pad in Fig. 4(f) can carry approximately $35 \mu\text{L}$ of water. Second, having a larger adhesion area implies the adhesion force can be better distributed to counteract the destabilizing torques due to gravity and leg contact forces.

We install the adhesion pad on a static robot model and conduct adhesion experiments on inverted and vertical surfaces. Fig. 5 and Supplementary Video 1 show pulling experiments on an inverted surface. A thread is attached to the base of the adhesion pad. We drop water on the adhesion pad, attach the robot inverted to an acrylic surface, and manually pull the thread to the left (Fig. 5(a) and (b)). On dry and wet surfaces, the robot remains attached while sliding to the left with speeds of 0.6 cm/s and 1.2 cm/s, respectively. Further, we conduct pulling experiments on a vertical acrylic surface (Fig. 6 and Supplementary Video 1). The pulling speeds on dry (Fig. 6(a)) and wet (Fig. 6(b)) surfaces are 0.7 cm/s and 0.9 cm/s, respectively. These experiments show that this adhesion design is feasible for inverted and vertical locomotion in insect-scale robots.

Further, we demonstrate this adhesion mechanism is versatile on a wide range of surfaces through conducting vertical pulling experiments on dry stainless-steel (Fig. 7(a)), dry wood

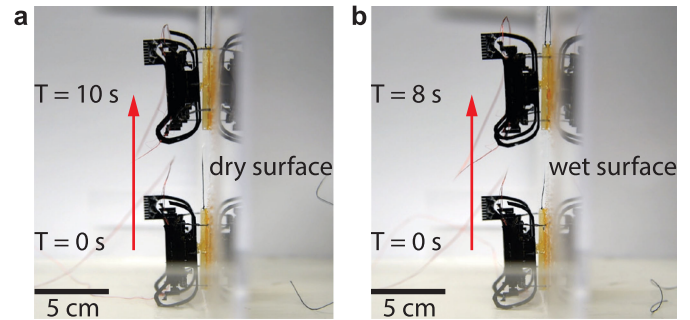


Fig. 6. Pulling demonstration on a vertical acrylic surface. (a) A robot model is pulled upward along a dry surface at a speed of 0.7 cm/s. (b) The same pulling experiment is conducted on a wetted surface at a speed of 0.9 cm/s.

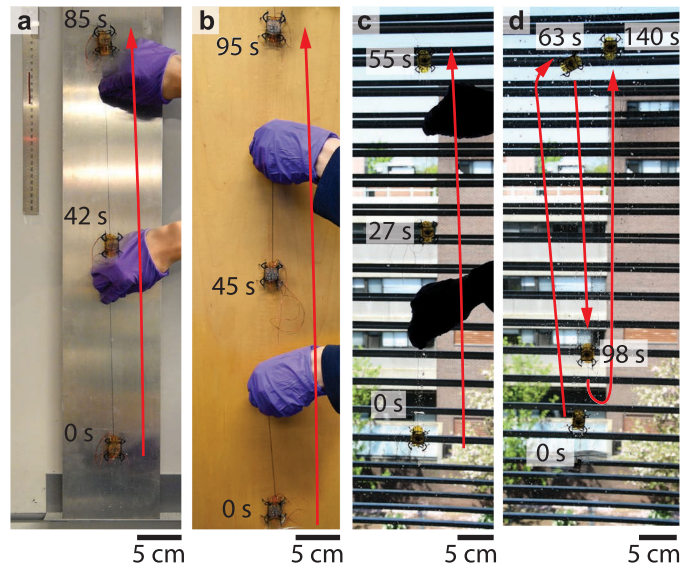


Fig. 7. Pulling demonstration on different vertical surfaces. (a)–(c), A robot model is pulled vertically along stainless steel, wood, and glass surfaces with an average speed of 0.8 cm/s, 0.8 cm/s and 1.6 cm/s, respectively. In (a)–(c), the surfaces are dry. (d) The robot model is pulled along a wetted glass surface at 1.8 cm/s. The robot remains attached during turning and vertical motion.

(Fig. 7(b)), dry and wet glass (Fig. 7(c) and (d)) surfaces. On a dry stainless-steel surface, the robot is pulled upward 65 cm in 85 seconds. On dry wood (Fig. 7(b)) and glass (Fig. 7(c)) surfaces, the robot maintains adhesion for 75 and 90 cm in 95 and 55 seconds, respectively. On these surfaces, the average pulling speeds are 0.8 cm/s, 0.8 cm/s, and 1.6 cm/s, respectively. In these experiments on dry surfaces, the water film leaves a water trace along the robot locomotion path and gradually thins out. This water film thinning causes a reduction of adhesion force and an increase of friction, and these ultimately lead to robot detachment. On these dry surfaces, the robot can be pulled approximately 100 cm before experiencing a detachment failure. In contrast, the robot can move on a wetted surface indefinitely (Fig. 7(d)) because the water film replenishes continuously. Fig. 7(d) shows the robot pulled to move 250 cm in 140 second on a wetted glass, and it is also pulled to make two 180° turns in this experiment. These experiments are shown in Supplementary Video 2.

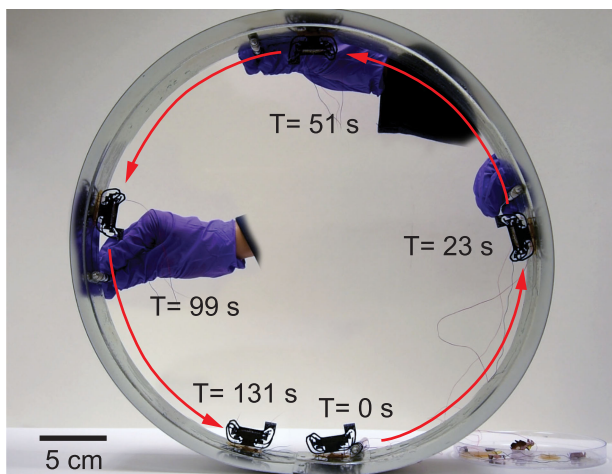


Fig. 8. Pulling demonstration on a circular track that has a 50 cm diameter. The robot is pulled along the inner face of a circular track at an average speed of 1.2 cm/s. This demonstration shows the adhesion mechanism can work on smooth surfaces of arbitrary incline angles.

In addition to moving on inverted and vertical surfaces, we demonstrate that the robot model can move along a curved stainless-steel surface using this adhesion mechanism. Fig. 8 and Supplementary Video 3 show a pulling experiment on a circular stainless steel track that has a diameter of 50 cm. The robot makes a complete turn in 135 seconds at an average speed of 1.2 cm/s. This experiment shows this compliant adhesion mechanism can adhere to surfaces of any inclined angle and the changing torque due to gravity at different orientations is passively compensated.

D. Demonstration of Robot Locomotion on Inverted and Inclined Surfaces

Here we demonstrate inverted climbing, turning, and inclined climbing using a HAMR. The robot is a 4.5 cm long, 1.4 g (13.7 mN) quadruped with a payload capacity of 2.9 g (28.4 mN). Each leg has two independently actuated DOFs corresponding to fore-aft (swing) and vertical (lift) leg motion. These DOFs are driven by piezoelectric bimorph bending actuators [24] that are controlled with AC voltage signals using a simultaneous drive configuration described by Karpelson *et al.* [25]. Doshi *et al.* [22] provides a more detailed description of this platform. We attach the larger adhesion pad (Fig. 4(f)) to the robot chassis. Fig. 9(a) shows a top view composite image of the robot climbing inverted on a dry acrylic surface. The robot moves 12 cm in 36 seconds with an average speed of 0.3 cm/s. It uses a 1 Hz trot gait that is originally designed for moving on level ground. The red trajectory in Fig. 9(a) shows the tracked COM motion, and Fig. 9(c) shows its forward displacement as a function of time. This experiment is also shown in the upper panel of Supplementary Video 4.

The robot can also climb inverted on a wetted acrylic surface using the same gait and adhesion pad. Fig. 9(b) shows the side view images of the robot climbing on a wet acrylic surface. The robot moves 4 cm in 38 seconds with an average speed of 0.1 cm/s, approximately three times slower than inverted climbing on a dry surface. This substantial speed reduction is

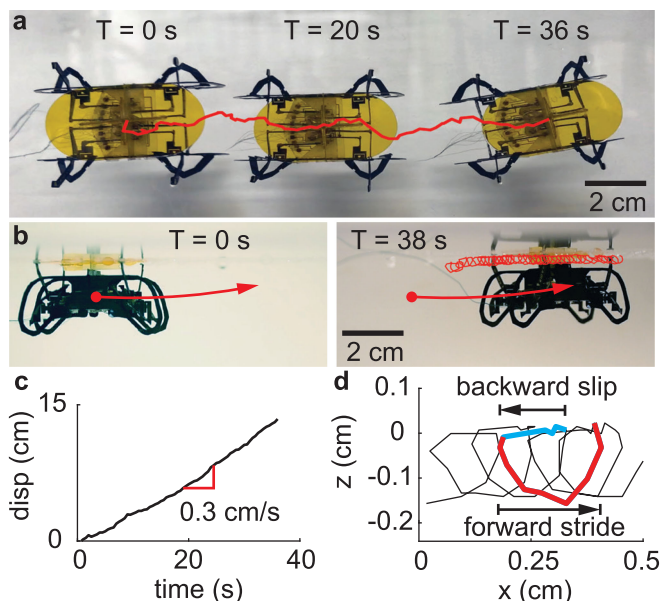


Fig. 9. Demonstration of inverted locomotion. (a) Top view composite image of a robot walking inverted on a dry surface at a speed of 0.3 cm/s for 36 seconds. The red line shows the tracked robot COM trajectory. (b) Side view images showing a robot walking inverted on a wetted surface at a speed of 0.1 cm/s for 38 seconds. The red line shows the robot's front left leg trajectory. (c) Tracked robot displacement that corresponds to the experiment shown in (a). (d) Zoomed-in robot foot trajectory that corresponds to the experiment shown in (b). The robot foot slips backward before lifting off the surface. This implies the wetted surface reduces contact friction at the robot feet, which causes backward slip and consequently a substantial reduction of walking speed.

due to the reduced friction at the robot feet. The red curve in Fig. 9(b) shows the tracked trajectory of the robot's left front leg. Fig. 9(d) zooms into four leg stride cycles and highlights one of the four cycles. The horizontal segment (blue colored) indicates foot backward slip. As the robot foot pushes against the acrylic surface, the water film reduces contact friction and causes the foot to slip backward. The circular segment (red colored) represents the robot lifting its leg, striding forward, and then pushing down to remake contact. In this experiment the backward slip is approximately 70% that of the forward stride, and consequently this causes the robot climbing speed to reduce by approximately three times. This experiment is shown in the bottom left panel of Supplementary Video 4.

Further, the robot can demonstrate turning on an inverted surface. Fig. 10(a) shows the robot making a 200° right turn followed by a 220° left turn in 48 seconds. Fig. 10(b) and (c) show the tracked robot orientation and angular velocity, and the red and blue regions indicate right and left turns, respectively. Using a 1 Hz turning gait, the robot right turn velocity is $7.2^\circ/\text{s}$, and it increases to $18.1^\circ/\text{s}$ when the turning gait frequency increases to 3 Hz. We command the robot to turn left with a 3 Hz turning gait, and it has an average turning speed of $23.6^\circ/\text{s}$ (blue regions in Fig. 10(d)). The turning experiment is shown in the bottom right panel of Supplementary Video 4.

Compared to a previous study [9] that uses electrostatic adhesion, this adhesion design has several advantages. First, the average inverted climbing speed (compared to supplemental

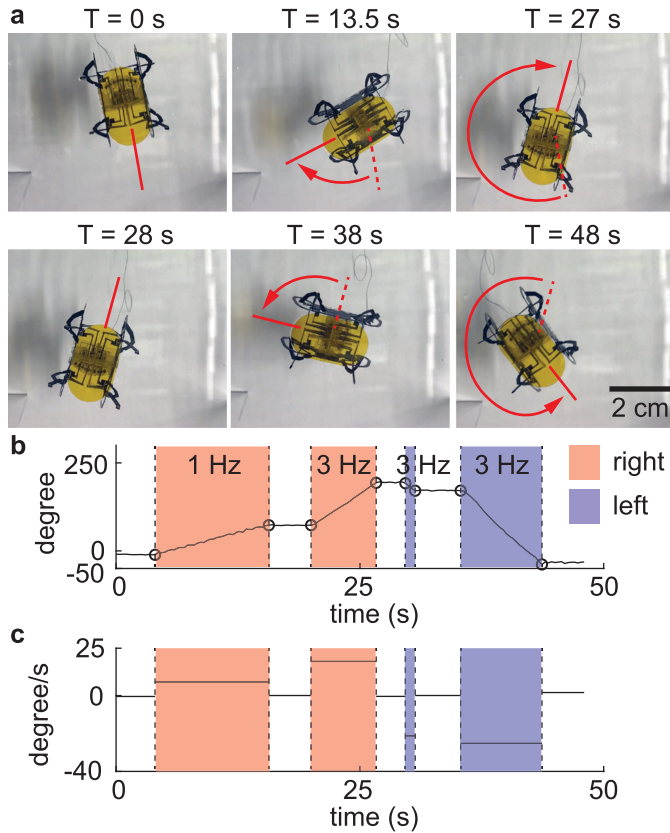


Fig. 10. Demonstration of inverted turning maneuvers. (a) An image sequence that shows robot right and left turn maneuvers. (b) Tracked robot orientation as a function of time. The red and blue colored regions represent right and left turns, respectively. (c) Robot turning velocity as a function of time. The turning speed is obtained by calculating the average speed between the marked events (black colored circles) in (b).

movie 2 in [9]) is improved by a factor of approximately four and the turning speed is increased by a factor of 13. Second, the previous study showed that inverted climbing through electrostatic adhesion cannot be sustained without sensing and feedback control. The previous study achieved a maximum number of 162 steps before having an attachment failure. In contrast, this design removes the need for repeated foot attachment and detachment, and the robot can move for up to a meter before the water film thins out on a dry surface. Third, this capillary-based adhesion mechanism provides a natural restoring torque that rejects disturbances during climbing, and consequently the robot can adapt previous locomotion gaits (such as the trot) for inverted locomotion. In contrast, the electrostatic-based method [9] requires careful analysis of the robot COM movement and a custom designed tri-pedal gait for inverted climbing. Finally, as shown in Fig. 7, this capillary-based adhesion mechanism can be used for locomotion on many surfaces such as stainless steel, wood, glass, and acrylic. The electrostatic approach requires high voltage sources and it has only been demonstrated on conductive surfaces. These advantages make capillary adhesion an attractive design for insect-scale climbing robots.

However, the current design has a shortcoming compared to the electrostatic adhesion mechanism [9]. While having a

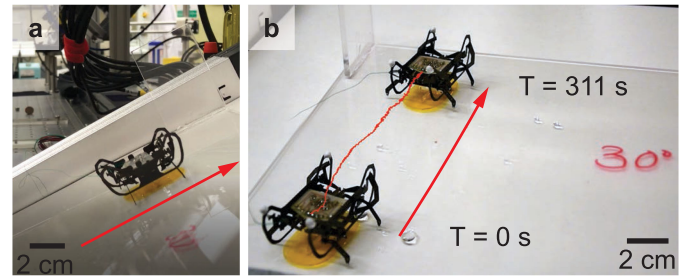


Fig. 11. Demonstration of robot climbing on a 30° incline. (a) A side view image showing the robot climbs on a 30 degree inclined acrylic surface. (b) The robot climbs 13 cm in 311 seconds with an average speed of 0.04 cm/s.

low friction force enables simultaneous adhesion and sliding, it becomes problematic for locomotion on vertical surfaces. This robot cannot climb on smooth vertical surfaces as the robot feet cannot generate sufficient friction to overcome gravity. Through experiments, we find that the robot cannot climb an acrylic surface with an incline angle larger than 40°. Here we demonstrate the robot can climb a 30° inclined dry acrylic surface. Fig. 11(a) shows a side view image of the climbing experiment. Fig. 11(b) shows the robot climbs 12.5 cm in 311 seconds with an average speed of 0.04 cm/s. This climbing speed is approximately 10 times slower than that of inverted climbing because of foot-slippage. In this experiment, the robot uses a 1 Hz trot gait and it does not require devices such as a passive tail [23] to maintain climbing stability. This experiment is shown in Supplementary Video 5.

IV. CONCLUSION

In this study, we propose a novel adhesion method based on capillary and lubrication effects. We derive analytical models and conduct experiments to show this adhesion method can generate a large normal adhesion force and a small friction force. We design a 47 mg adhesion mechanism and install it into a 1.4 g quadrupedal robot. We demonstrate the robot can climb and make turns on an inverted surface with average speeds of 0.3 cm/s and 23.6°/s, respectively. Further, the robot can climb a 30° acrylic incline at a speed of 0.04 cm/s.

The main advantage of this design is that it eliminates the need of repeated attachment and detachment between the attaching mechanism and the desired surface. Since the robot remains attached while it moves along a surface, it does not require special climbing gaits that consider destabilizing torques or disturbances. Further, this passive adhesion design is light-weight and easy to fabricate, and it can adhere to a wide range of non-water-absorbing surfaces such as glass, plastic, stainless steel, and wood. Table II compares this adhesion design with three existing methods, and this design is the only method that does not require repeated attachment and detachment during robot locomotion. As shown in the second and third columns of Table II, this design uncouples robot locomotion and adhesion by providing a large adhesive force and a small friction force. The capillary force attaches a robot to a surface, and the small friction force does not impede robot locomotion along the surface. This

TABLE II
COMPARISON OF ADHESION METHODS

Adhesion method	F_N/F_g	F_f/F_g	Advantages and disadvantages
Microspines and gecko adhesive [23]	small	large	+ light weight device – cannot climb on inverted surfaces
Electrostatic adhesion [9] [11] [18]	large	large	+ tunable adhesion force – needs well planned gaits – sensitive to surface conductive properties – requires high voltage
Vacuum-based adhesion [14] [15]	large	large	+ strong adhesion force – requires a pump
Capillary adhesion	large	small	+ allows sliding adhesion + light weight device + no sensing needed – need to carry water

adhesion design is particularly suitable for micro-scale robots that have limited payload, sensing, and control. Capillary effects pose both challenges and opportunities for insect-scale robots, and they further enable novel locomotive capabilities such as climbing, walking on the water surface [26], and aerial-aquatic transitions [27].

Despite having these advantages, our robot cannot demonstrate vertical climbing on smooth surfaces due to limited friction at the robot feet. This is not a limitation of the adhesion mechanism because we aim to minimize friction to allow simultaneous adhesion and sliding. This challenge can be solved by incorporating other adhesion mechanisms such as micro-spines or electrostatic adhesion in the robot feet. We envision that climbing friction will be generated by the robot feet while the adhesion pad provides an adhesive normal force.

For inverted locomotion on a smooth surface such as glass, we show 35 μL of water allows a moving distance of approximately 1 meter. To travel longer distances, we need to incorporate a water-supplying micro-fluidic circuit or design adhesion pads that can carry water as a robot moves across a surface. If the robot carries 0.35 g (out of 2.9 g of net payload) of water, then it would be able to climb inverted for 10 meters. Future experiments can evaluate how surface roughness influences water film thinning and reduces net travel distance. In addition, our analysis and experiment showed the adhesion and friction forces are related to the water film thickness. Future work that can supply water to the adhesion pad can further demonstrate tunable adhesion through controlling the water film thickness. Achieving tunable adhesion and friction will further allow the adhesion pad to detach and reattach when a robot needs to move over a gap on a discontinuous surface.

REFERENCES

[1] T. Endlein and W. Federle, "On heels and toes: How ants climb with adhesive pads and tarsal friction hair arrays," *PLoS One*, vol. 10, no. 11, p. e0141269, 2015.
[2] K. Autumn *et al.*, "Adhesive force of a single gecko foot-hair," *Nature*, vol. 405, no. 6787, pp. 681–685, 2000.

[3] K. Autumn, A. Dittmore, D. Santos, M. Spenko, and M. Cutkosky, "Frictional adhesion: A new angle on gecko attachment," *J. Exp. Biol.*, vol. 209, no. 18, pp. 3569–3579, 2006.
[4] S. N. Gorb, "Uncovering insect stickiness: Structure and properties of hairy attachment devices," *Amer. Entomologist*, vol. 51, no. 1, pp. 31–35, 2005.
[5] W. Federle, M. Riehle, A. S. Curtis, and R. J. Full, "An integrative study of insect adhesion: Mechanics and wet adhesion of pretarsal pads in ants," *Integrative Comparative Biol.*, vol. 42, no. 6, pp. 1100–1106, 2002.
[6] S. Kim, A. T. Asbeck, M. R. Cutkosky, and W. R. Provancher, "SpinybotII: climbing hard walls with compliant microspines," in *Proc. 12th Int. Conf. Adv. Robotics*, 2005, pp. 601–606.
[7] S. Kim, M. Spenko, S. Trujillo, B. Heyneman, V. Mattoli, and M. R. Cutkosky, "Whole body adhesion: Hierarchical, directional and distributed control of adhesive forces for a climbing robot," in *Proc. IEEE Int. Conf. Robot. Autom.*, Apr. 2007, pp. 1268–1273.
[8] G. A. Lynch, J. E. Clark, P. C. Lin, and D. E. Koditschek, "A bioinspired dynamical vertical climbing robot," *Int. J. Robot. Res.*, vol. 31, no. 8, pp. 974–996, 2012.
[9] S. D. de Rivaz, B. Goldberg, N. Doshi, K. Jayaram, J. Zhou, and R. J. Wood, "Inverted and vertical climbing of a quadrupedal microrobot using electroadhesion," *Sci. Robot.*, vol. 3, no. 25, 2018, Paper eaau3038.
[10] Y. Zhang, L. Ge, J. Zou, H. Xu, and G. Gu, "A multimodal soft crawling-climbing robot with the controllable horizontal plane to slope transition," in *Proc. IEEE/RSJ Int. Conf. Intell. Robots Syst.*, 2019, pp. 3343–3348.
[11] H. Wang, A. Yamamoto, and T. Higuchi, "A crawler climbing robot integrating electroadhesion and electrostatic actuation," *Int. J. Adv. Robot. Syst.*, vol. 11, no. 12, p. 191, 2014.
[12] W. Shen, J. Gu, and Y. Shen, "Proposed wall climbing robot with permanent magnetic tracks for inspecting oil tanks," in *IEEE Int. Conf. Mechatronics Autom.*, 2005, vol. 4, pp. 2072–2077.
[13] M. Eich and T. Vögele, "Design and control of a lightweight magnetic climbing robot for vessel inspection," in *Proc. 19th Mediterranean Conf. Control Autom.*, 2011, pp. 1200–1205.
[14] B. Bridge, C. Hillenbrand, D. Schmidt, and K. Berns, "CROMSCI: Development of a climbing robot with negative pressure adhesion for inspections," *Ind. Robot. Int. J.*, 2008.
[15] T. Miyake, H. Ishihara, and M. Yoshimura, "Basic studies on wet adhesion system for wall climbing robots," in *Proc. IEEE/RSJ Int. Conf. Intell. Robots Syst.*, 2007 pp. 1920–1925.
[16] B. He *et al.*, "Wet adhesion inspired bionic climbing robot," *IEEE/Asme Trans. Mechatronics*, vol. 19, no. 1, pp. 312–320, Feb. 2013.
[17] R. Liu, R. Chen, H. Shen, and R. Zhang, "Wall climbing robot using electrostatic adhesion force generated by flexible interdigital electrodes," *Int. J. Adv. Robot. Syst.*, vol. 10, no. 1, p. 36, 2013.
[18] G. Gu, J. Zou, R. Zhao, X. Zhao, and X. Zhu, "Soft wall-climbing robots," *Sci. Robot.*, vol. 3, no. 25, 2018, Paper eaat2874.
[19] J. W. M. Bush, 2014. 18.357 Interfacial Phenomena, Fall 2010. [Online]. Available: <http://math.mit.edu/~bush/wordpress/wp-content/uploads/2018/02/18.357-LecNotes-2010.pdf>
[20] A. Hennig *et al.*, "Contact angle hysteresis: Study by dynamic cycling contact angle measurements and variable angle spectroscopic ellipsometry on polyimide," *Langmuir*, vol. 20, no. 16, pp. 6685–6691, 2004.
[21] B. Medgyes, B. Illès, and L. Gál, "Measurements of water contact angle on FR4 and polyimide substrates relating electrochemical migration," in *Proc. 36th Int. Spring Seminar Electron. Technol.*, May 2013, pp. 157–160.
[22] N. Doshi *et al.*, "Model driven design for flexure-based microrobots," in *Proc. IEEE/RSJ Int. Conf. Intell. Robots Syst.*, Sep. 2015, pp. 4119–4126.
[23] B. F. Seitz *et al.*, "Bio-inspired mechanisms for inclined locomotion in a legged insect-scale robot," in *Proc. IEEE Int. Conf. Robot. Biomimetics*, Dec. 2014, pp. 791–796.
[24] N. T. Jafferis, M. J. Smith, and R. J. Wood, "Design and manufacturing rules for maximizing the performance of polycrystalline piezoelectric bending actuators," *Smart Mater. Struct.*, vol. 24, no. 6, 2015, Art. no. 065023.
[25] M. Karpelson, G. Y. Wei, and R. J. Wood, "Driving high voltage piezoelectric actuators in microbotic applications," *Sensors Actuators A: Physical*, vol. 176, pp. 78–89, 2012.
[26] Y. Chen, N. Doshi, B. Goldberg, H. Wang, and R. J. Wood, "Controllable water surface to underwater transition through electrowetting in a hybrid terrestrial-aquatic microrobot," *Nature Commun.*, vol. 9, no. 1, pp. 1–11, 2018.
[27] Y. Chen *et al.*, "A biologically inspired, flapping-wing, hybrid aerial-aquatic microrobot," *Sci. Robot.*, vol. 2, no. 11, 2017, Paper eaao5619.